RSC Advances

PAPER

Cite this: *RSC Adv.*, 2020, **10**, 15375

Comb-shaped cardo poly(arylene ether nitrile sulfone) anion exchange membranes: significant impact of nitrile group content on morphology and properties†

Ao Nan Lai,* Peng Cheng Hu, Rong Yu Zhu, Qi Yin and Shu Feng Zhou*

A series of comb-shaped cardo poly(arylene ether nitrile sulfone) (**CCPENS-*x***) materials were synthesized by varying the content of nitrile groups as anion exchange membranes (AEMs). The well-designed architecture of cardo-based main chains and comb-shaped C10 long alkyl side chains bearing imidazolium groups was responsible for the clear microphase-separated morphologies, as confirmed by atomic force microscopy. The ion exchange capacity (IEC) of the AEMs ranged from 1.56 to 1.65 meq. g^{-1}. With strong dipole interchain interactions, the effects of nitrile groups on the membrane morphology and properties were investigated. With the nitrile group content increasing from CCPENS-0.2 to CCPENS-0.8, **CCPENS-*x*** revealed larger and more interconnected ionic domains to form more efficient ion-transport channels, thus increasing the corresponding ionic conductivity from 25.8 to 39.5 mS cm^{-1} at 30 °C and 58.6 to 83 mS cm^{-1} at 80 °C. Furthermore, **CCPENS-*x*** with a higher content of nitrile groups also exhibited lower water uptake (WU) and swelling ratio (SR), and better mechanical properties and thermal stability. This work presents a promising strategy for enhancing the performance of AEMs.

Received 25th February 2020
Accepted 7th April 2020

DOI: 10.1039/d0ra01798a

rsc.li/rsc-advances

Introduction

As a clean and highly efficient renewable energy conversion device, the fuel cell has attracted considerable attention in the last decade.[1–3] Of various fuel cell types, alkaline electrolyte membrane fuel cells (AEMFCs) hold particular attention with their merits of faster oxygen reduction reaction kinetics[4] and their potential to use non-precious metal catalysts (*e.g.*, metal oxides[5] and transition metals[6,7]), which could significantly reduce the cost of production. As a key component of AEMFCs, anion exchange membranes (AEMs) have an important effect on the whole electrochemical performance of fuel cells. However, the existing AEMs still suffer from some challenges such as the trade-off between dimensional stability and conductivity, and the poor alkaline durability, which delayed the large-scale commercialization of AEMFCs.[8–10]

To achieve high-performance AEMs, materials such as poly(phenylene oxide),[11] poly(styrene),[12] poly(ionic liquid),[13] poly(ether imide),[14] polyolefin,[15] poly(arylene ether ketone)[16] and poly(arylene ether sulfone)[17,18] were modified by incorporating with hydroxide ion exchange groups such as imidazolium,[19] quaternary ammonium,[14,15] guanidinium,[20] pyridinium,[21] morpholinium,[22] piperidinium,[11,23] pyrrolidinium,[18,24] phosphonium[25] and metal ions,[26] *etc.* Furthermore, the microstructure of the AEMs also plays a key role in membrane's properties. Recent studies show that the construction of hydrophilic–hydrophobic microphase separation is an effective strategy for forming continuous and wide ion pathways and improving ionic conductivity. Microphase separation can be achieved in block-type AEMs[27–31] (with ion exchange groups located on block main chains) and side-chain-type AEMs[32–36] (with ion exchange groups grafted at pendant side-chains).

In addition, inspired by Nafion® structure, many researchers were interested in comb-shaped AEMs, where ion exchange groups grafted or beside on the long flexible side chains.[37–41] In these comb-shaped AEMs, nano-scale ionic clusters were observed to form distinct microphase separation structures. Furthermore, the dimensional and alkaline stability of these AEMs could also be elevated due to the hydrophobicity and steric hindrance effect of long side chains. For instance, Zhuang *et al.* designed and synthesized a series of comb-shaped polysulfone-based AEMs with long alkyl side chains. The obtained AEMs exhibit ordered ion-aggregating structures and OH^- conducting highways, high conductivity, suppressed water swelling, excellent mechanical and chemical stabilities.[42] However, in most cases, researchers still used the method of increasing the number of ion exchange groups in the polymer matrix to further enhance the microphase separation between hydrophilic ionic clusters and hydrophobic domains.[43,44] These AEMs also tended to swell

College of Chemical Engineering, Huaqiao University, Xiamen 361021, PR China. E-mail: aonanlai@hqu.edu.cn; szhou@hqu.edu.cn

† Electronic supplementary information (ESI) available. See DOI: 10.1039/d0ra01798a

seriously and weaken the dimensional stability while at high level of ion exchange capacity (IEC).

In this study, a series of comb-shaped cardo AEMs was designed and synthesized using 1-decyl-2-methylimidazole (DIm, containing C10 long alkyl chain) as the quaternization reagent and poly(arylene ether nitrile sulfone) (PENS) as the polymer backbones. The bulky cardo groups of phenolphthalein monomers were introduced to fence off each chain and increase the free volume for hydroxide transmission.[45] The nitrile groups suspended on backbones possess a high dipole moment of ~3.9 debye.[46] With strong dipole interchain interactions, the effects of nitrile groups on the microphase separation and properties of AEMs could not be neglected.[47,48] Thus in this work, we tried to adjust the microphase separation by regulating the content of nitrile groups instead of cationic groups. Then the comb-shaped cardo poly(arylene ether nitrile sulfone) AEMs with varied content of nitrile groups were prepared and characterized. The essential point of this work is to investigate the effects of nitrile groups on the morphology and properties of the comb-shaped cardo PENS AEMs.

Experimental

Materials

Bis(4-fluorophenyl)sulfone (FPS) (99%, TCI, Japan), *o*-Cresolphthalein (oCPH) (99%, TCI, Japan), 2,6-difluorobenzonitrile (DFBN) (99%, Aladdin, China), *N*-bromosuccinimide (NBS) (99%, Aladdin, China) and DIm (97%, Sigma-Aldrich, St. Louis, MO) were used as received. Toluene and *N*,*N*-dimethylacetamide (DMAc) (99.8%, Aladdin, China) were stirred over CaH_2 for 24 h, then distilled under reduced pressure and stored over 4 Å molecular sieves. Benzoyl peroxide (BPO) (97%, Alfa, China) was purified by recrystallizing from chloroform. All other reagents were supplied from Shanghai Sinopharm Chemical Reagent Co., Ltd (China) and used without further purification.

Preparation of anion exchange membranes

Synthesis of cardo poly(arylene ether nitrile sulfone) (CPENS-*x*). The precursor **CPENS-*x*** was synthesized by nucleophilic substitution polycondensation (Scheme 1), where *x* represents the feed molar ratio of DFBN to oCPH. A typical procedure for the synthesis of CPENS-0.6 is detailed as follows: DFBN (6 mmol, 0.835 g), FPS (4 mmol, 1.017 g), oCPH (10 mmol, 3.464 g), K_2CO_3 (25 mmol, 3.455 g), DMAc (25 mL) and toluene (10 mL) were placed into a 150 mL three-necked round-bottomed flask equipped with a Dean–Stark apparatus, a magnetic stirrer, and a nitrogen inlet and outlet. The reaction was conducted at 140 °C for 4 h and then slowly increased to 160 °C for another 20 h after removing the toluene. During this period, the reaction mixture was diluted by additional 5 mL of DMAc. After the reaction, the solution was cooled to room temperature (RT) and dripped into 500 mL of an aqueous methanol solution (methanol/deionized water = 1/1, v/v) to yield a white solid precipitate. Subsequently, the product was kept stirring in the aqueous methanol solution for another 5 h, filtrated, purified by Soxhlet extraction with methanol for 12 h and dried at 80 °C under vacuum for 24 h.

Bromination of CPENS-*x*. The **CPENS-*x*** was brominated in 1,1,2,2-tetrachloroethane (TCE) by using NBS as the bromination agent and BPO as the initiator (Scheme 1). A typical procedure is as follows. 1.0 g of CPENS-0.6 (containing 4.073 mmol of $-CH_3$) was dissolved in 20 mL of TCE under stirring, then 0.870 g of NBS (4.888 mmol) and 0.059 g of BPO (0.244 mmol) were charged. The bromination reaction was conducted at 85 °C for 5 h under stirring in N_2 atmosphere. After cooling to RT, the mixture solution was dripped into 300 mL methanol solution to yield a yellow solid precipitate. The product was collected by filtration, Soxhlet extracted with methanol for 12 h and dried at 60 °C under vacuum for 24 h. The brominated polymers are termed **BCPENS-*x***, where B denotes the bromination reaction.

Synthesis of comb-shaped cardo poly(arylene ether nitrile sulfone) (CCPENS-*x*) and membrane formation. **CCPENS-*x*** was prepared *via* the nucleophilic substitution reaction of **BCPENS-*x*** with DIm (Scheme 1). A typical procedure is as follows. 1 g of BCPENS-0.6 (containing 2.620 mmol of $-CH_2Br$) was dissolved in 20 mL dimethyl sulfoxide (DMSO) under stirring to form a homogeneous solution. Then 777 μL of DIm (3.144 mmol) was added into the reaction slowly. The imidazolium functionalization was conducted at 45 °C for 24 h. Afterwards, the solution was filtered through a 0.45 μm PTFE membrane filter, casted onto a flat and clean glass plate and dried at 60 °C for 48 h under vacuum to form a membrane. The obtained membranes were immersed in 1 M KOH solution to convert the Br^- to OH^-. Finally, the AEMs were stored in deionized water for more than 24 h before use.

Characterization and measurement

Detailed instrumental analyses and measurements for the FT-IR and ^1H NMR spectra, gel permeation chromatography (GPC), IEC, swelling ratio (SR), water uptake (WU), atomic force microscopy (AFM), scanning electron microscopy (SEM), ionic conductivity (σ), mechanical property, thermal and alkaline stability are described in detail in Section S1 (ESI).†

Results and discussion

Synthesis and characterization of CPENS-*x* and BCPENS-*x*

CPENS-*x* with different contents of nitrile groups was synthesized by polycondensation with various feed molar ratios of DFBN to FPS. Fig. S1 (ESI)† shows the ^1H NMR spectrum of CPENS-0.6. In the aromatic regions, peaks around 7.65, 7.78 and 8.02 ppm (h, j, i, k in Fig. S1†) are assigned to the aromatic protons of cardo groups. All the other aromatic protons on the main chains are well-assigned to the aimed polymer structure. The peak at 7.29 ppm is assigned to $CDCl_3$. The peaks around 2.15–2.25 ppm are associated with the chemical shifts of the benzylmethyl groups (a and a′ in Fig. S1†). The ratio of the integration of the protons on positions a′ and a gives $x = 0.60$, as shown in Table 1.

The synthesis of **BCPENS-*x*** was conducted in TCE using NBS as the bromination agent and BPO as the initiator. Fig. S2 (ESI)†

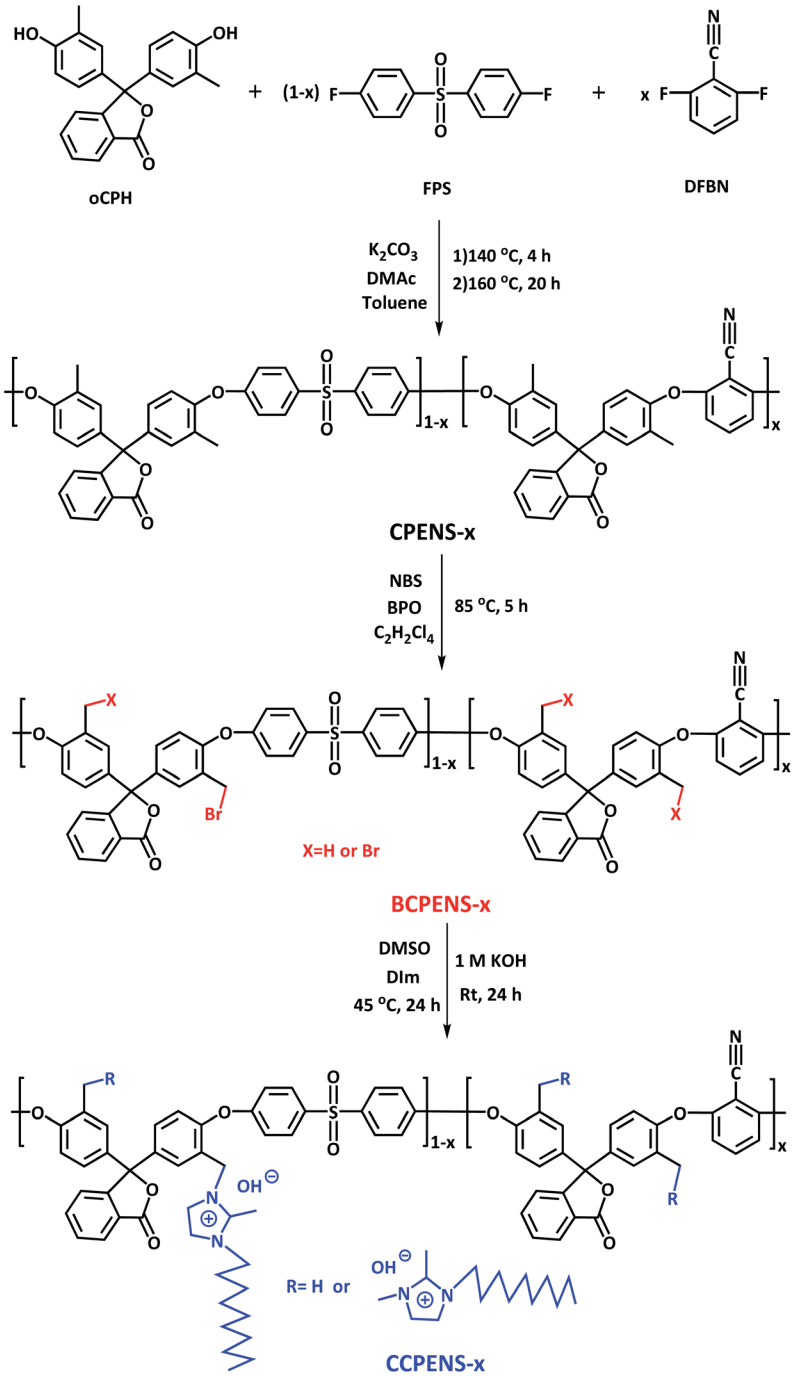

Scheme 1 Synthesis of CPENS-*x*, BCPENS-*x* and CCPENS-*x*.

shows the ^{1}H NMR spectrum of BCPENS-0.6. A comparison with CPENS-0.6 (Fig. S1, ESI†) reveals that new characteristic peaks corresponding to the chemical shifts of the bromomethyl groups appeared at 4.43–4.58 ppm (1 and 1′ in Fig. S2†), and the peaks assignable to the benzylmethyl groups (a and a′ in Fig. S2†) decreased in size. This confirms the successful synthesis of BCPENS-0.6. The bromomethylation degree of the **BCPENS-*x*** can be calculated from the ratio of the integral area of the brominated benzyl peaks (1 and 1′ in Fig. S2,† $-CH_2Br$, two protons) to the sum of unreacted benzylmethyl peaks (a and a′ in Fig. S2,† $-CH_3$, three protons) and the brominated benzyl peaks, as shown in Table 1. Moreover, the **BCPENS-*x*** show a high molecular weight (M_n > 55 kDa, Table 1) for membrane formation.

Membrane formation and FI-IR spectra

As shown in Scheme 1, **CCPENS-*x*** AEMs were synthesized by using **BCPENS-*x*** as the base polymers and DIm as the functional agent. Fig. S3 (ESI)† shows the ^{1}H NMR spectrum of CCPENS-0.6. The characteristic peaks of the methyl protons at

Table 1 Key properties of CPENS-*x* and BCPENS-*x*

	x						
CPENS-*x*	Theo.[a]	Cal.[b]	**BCPENS-*x***	Bromination degree[b] (%)	M_n[c] (kDa)	M_w[c] (kDa)	M_w/M_n[c]
CPENS-0.2	0.20	0.21	BCPENS-0.2	80.3	58.6	98.3	1.68
CPENS-0.4	0.40	0.38	BCPENS-0.4	81.8	55.2	101.5	1.84
CPENS-0.6	0.60	0.60	BCPENS-0.6	81.1	66.3	124.6	1.88
CPENS-0.8	0.80	0.79	BCPENS-0.8	83.5	67.4	115.1	1.71

[a] The theoretical value determined by feed monomer ratio. [b] The calculated value determined by ^{1}H NMR. [c] Determined by GPC analysis.

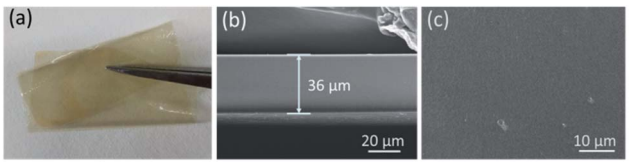

Fig. 1 (a) Photo, SEM images (b) cross-section and (c) surface of CCPENS-0.6.

2.55 ppm (H2) and the methylene protons at 7.00–7.10 ppm (H3 and H4) of the imidazolium ring, and the methylene protons at around 4.00 ppm (H5), 1.60 ppm (H6) and 1.15–1.35 ppm (H7–13) together with the methyl protons at 0.85 ppm (H14) of aliphatic chain, indicating the successful incorporation of DIm groups into the AEMs. Furthermore, a comparison with BCPENS-0.6 (Fig. S2†) shows that new peaks at 5.40–5.65 ppm (1 and 1′ in Fig. S3†) corresponding to Ar–CH_2–N protons appeared and the peaks at 4.43–4.58 ppm associated with the Ar–CH_2–Br protons disappeared mostly. This confirms the mostly conversion of BCPENS-0.6 to CCPENS-0.6.

The chemical structures of the **CCPENS-*x*** AEMs were further determined by FT-IR, as shown in Fig. S4 (ESI).† The characteristic peaks at 2231 cm^{-1} are assigned to the symmetric C–N stretching vibration of nitrile groups. The strong absorption bands at 1245 cm^{-1} are associated with the asymmetric C–O stretching vibrations of phenoxy groups. For CCPENS-0.6, the new broad bands around 3406 cm^{-1} are corresponding to the stretching vibrations of –OH bonds, and the characteristic bands at 1693 and 668 cm^{-1} are assignable to the vibration of imidazolium cations. Both ^{1}H NMR and FT-IR results confirm the successful preparation of **CCPENS-*x*** AEMs.

Furthermore, the appearance and SEM images of the CCPENS-0.6 membrane were also provided. As shown in Fig. 1a, the as-prepared membrane is flexible and transparent. The SEM images show that the membrane with a thickness of 36 μm is homogeneous and dense without any visible cracks (Fig. 1b and c).

IEC, WU and SR of the AEM

As a critical factor affecting the membrane properties, IEC represents the concentration of exchangeable ion groups in membrane matrix. As listed in Table 2, the theoretical IEC values between 1.75–1.92 meq. g^{-1} were calculated by the assumption that all benzyl bromide groups are quantitatively grafted with DIm groups and the bromide ions are totally exchanged with hydroxide ions. The experimental IEC values of **CCPENS-*x*** AEMs in the range of 1.56–1.65 meq. g^{-1} were measured by titration method and slightly lower than the corresponding theoretical IEC value. This is probably due to the high steric hindrance effect of long alkylene chain in DIm and the cardo groups in the main chains, which lead to incomplete quaternization reactions.

AEM with a suitable level of WU and SR is essential for both a valuable ionic conductivity and an acceptable mechanical strength. As shown in Fig. 2, the WU decreased slightly from 24.2% to 21.9% at 30 °C and 35.8% to 27.1% at 80 °C from CCPENS-0.2 to CCPENS-0.8, and the corresponding SR decreased from 7.8% to 6.8% at 30 °C and from 12.7% to 9.2% at 80 °C. For a better comparison of the WU in the **CCPENS-*x*** membranes, we also calculated the hydration numbers (λ). As shown in Table 2, λ for **CCPENS-*x*** is between 7.37–8.61 at 30 °C and 9.11–12.74 at 80 °C. In summary, both the WU, SR and λ of the **CCPENS-*x*** tend to decrease with increasing the nitrile group

Table 2 IEC, λ, mechanical properties and $T_{d\text{-}5\%}$ of CCPENS-*x*

	IEC (meq. g^{-1})		λ[c]					
AEMs	Theo.[a]	Exp.[b]	30 °C	60 °C	80 °C	Tensile strength (MPa)	Elongation at break (%)	$T_{d\text{-}5\%}$ (°C)
CCPENS-0.2	1.75	1.56	8.61	10.49	12.74	24.2 ± 0.4	4.8 ± 0.2	196.0
CCPENS-0.4	1.80	1.58	8.18	9.94	11.41	24.8 ± 0.5	5.5 ± 0.3	206.6
CCPENS-0.6	1.84	1.61	8.13	9.58	10.1	26.5 ± 0.5	7.3 ± 0.4	220.4
CCPENS-0.8	1.92	1.65	7.37	8.61	9.11	27.6 ± 0.6	6.1 ± 0.4	232.2

[a] Calculated from the polymer composition and the bromination degree of **BCPENS-*x***. [b] Estimated by back titration. [c] Calculated from the WU and the Exp. IEC of the AEMs.

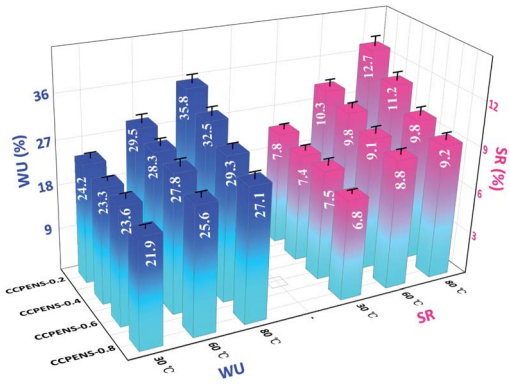

Fig. 2 WU and SR of **CCPENS-*x*** AEMs at different temperatures.

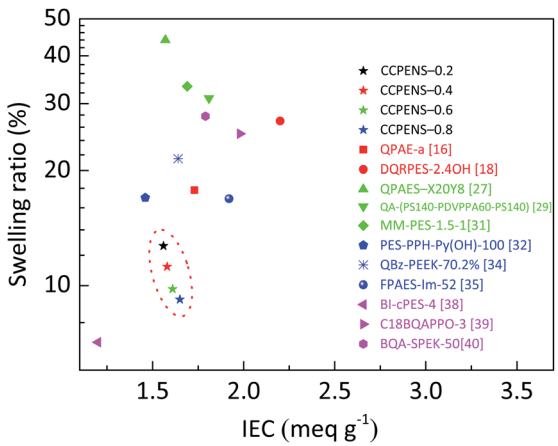

Fig. 3 Swelling ratio of the AEMs as a function of IEC at 80 °C.

content. It is considered that the nitrile groups with strong polarity could strengthen the intra/interchain interaction and thus restrict the water absorption and membrane swelling.[46,49]

A comparison of the swelling ratio of **CCPENS-*x*** membranes with some random-type AEMs,[16,18] block-type AEMs,[27,29,31] side-chain-type AEMs[32,34,35] and comb-shaped AEMs[38–40] is shown in Fig. 3, as a function of IEC at 80 °C. The **CCPENS-*x*** membranes displayed a lower swelling ratio at a moderate level of IEC, which reveals that the AEMs have good dimensional stabilities and anti-swelling properties. Besides the nitrile groups, the membrane structure of the comb-shaped side chains and cardo-based main chains also plays an important role. The long carbon chains of the DIm groups together with the bulky cardo groups can provide an integrated steric hindrance effect and fence off each chain to construct some inter-chain spacing, in which the water molecules could be placed and trapped.[50,51]

Ionic conductivity (σ), apparent activation energy (E_a) and membrane morphology

As a critical property of AEMs, the ionic conductivity of **CCPENS-*x*** membranes was investigated as a function of temperature. As shown in Fig. 4a, the conductivity increases along with the raising temperature due to the promoted water mobility. Moreover, with the nitrile group content increased from

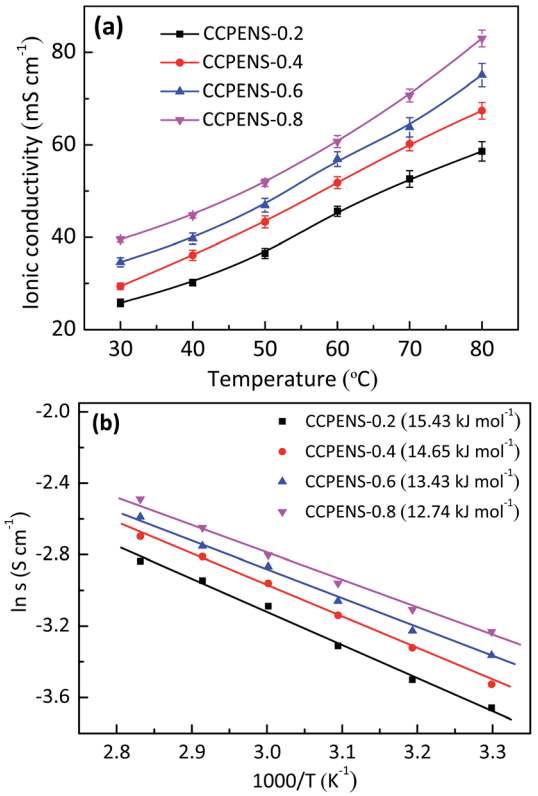

Fig. 4 (a) Temperature dependence of ionic conductivity and (b) Arrhenius plots of **CCPENS-*x*** AEMs.

CCPENS-0.2 to CCPENS-0.8, the conductivity improves from 25.8 to 39.5 mS cm^{-1} at 30 °C and from 58.6 to 83 mS cm^{-1} at 80 °C. To investigate the ionic conduction behavior more deeply, we displayed the ionic conductivity data as the Arrhenius plot and found it is almost linear. Then the apparent activation energy (E_a) was calculated by $E_a = -R \times b$, where R represents the gas constant (8.314 J mol^{-1} K^{-1}) and b refers to the slope of the ln σ *vs.* 1000/T curves.[18] As shown in Fig. 4b, the E_a of **CCPENS-*x*** membrane was estimated and decreased from 15.43 to 12.74 kJ mol^{-1} by increasing the nitrile group content. Furthermore, the E_a values of **CCPENS-*x*** are much lower than that of the reported comb-shaped membranes.[38,40]

The close relationship between ionic conduction behavior and nitrile group content would be attributed to the difference in membrane morphology. As shown in Fig. 5a and b of the AFM images, the darker and cluster-like regions are ascribed to the soft hydrophilic ionic domains, and the brighter regions are ascribed to the hard hydrophobic polymer chains.[37] It could be observed that both CCPENS-0.2 and CCPENS-0.8 exhibited clear hydrophilic/hydrophobic microphase-separated morphologies. Besides, CCPENS-0.8 exhibited more distinct phase-separated morphology and formed larger and more interconnected ionic domains than CCPENS-0.2. The clear microphase separation of **CCPENS-*x*** can be attributed to the well-designed architecture of cardo-based main chains and comb-shaped C10 long alkyl side chains bearing imidazolium groups.[37,41] Moreover, with the nitrile group content increased, the intra/intermolecular

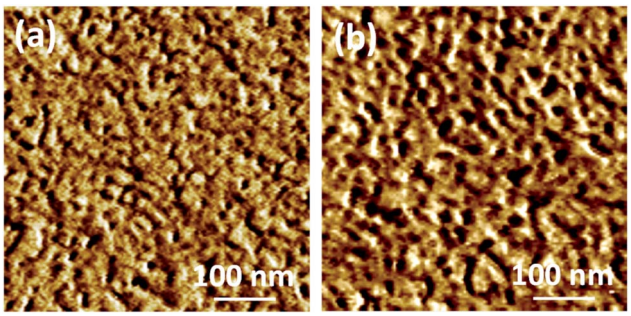

Fig. 5 AFM phase images of (a) CCPENS-0.2 and (b) CCPENS-0.8 membranes.

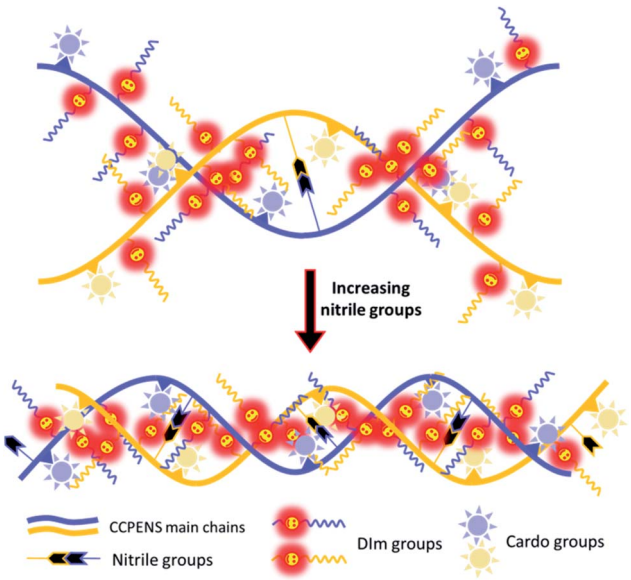

Scheme 2 Schematic process of morphological changes for CCPENS-*x*.

interaction is obviously enhanced and the polymer main chains are more strongly aligned (Scheme 2). As a result, defined spaces could be formed between the chains for ion transportation, where the imidazolium functional groups can be assemble and concentrated to form larger and more interconnected ionic domains, resulting in more efficient ion transport channels and lower E_a values together with higher conductivities.

Furthermore, **CCPENS-*x*** membranes are found to have superb ratios of conductivity to swelling ratio at 80 °C. Fig. 6 shows the comparison of swelling ratio and ionic conductivity of **CCPENS-*x*** with some recently reported AEMs at 80 °C. On the top-left portion of the graph, **CCPENS-*x*** with more nitrile groups showed lower swelling ratio and higher conductivity. This suggests that it is an effective method to improve conductivity and restrain dimensional swelling by regulating the content of nitrile groups in **CCPENS-*x*** AEMs in this work.

Mechanical property and thermal stability

Desirable mechanical properties of the AEMs are required for their practical applications. Table 2 presents the mechanical

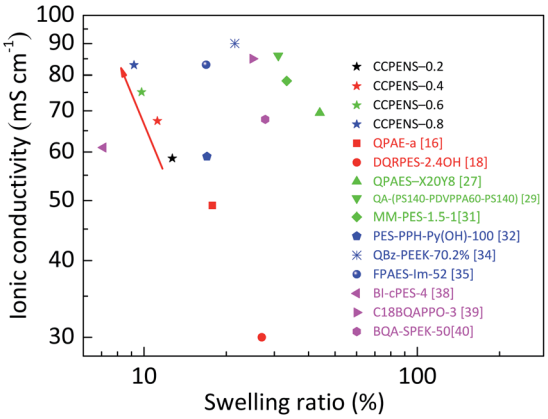

Fig. 6 Ionic conductivity of the AEMs as a function of swelling ratio at 80 °C.

properties of **CCPENS-*x***. Benefitted from the low levels of swelling ratio, **CCPENS-*x*** membranes under the hydrated condition exhibited good tensile strength and elongation at break in the range of 24.2–27.6 MPa and 4.8–7.3%, respectively. With nitrile group content increased from CCPENS-0.2 to CCPENS-0.6, the **CCPENS-*x*** showed a slight improvement for both tensile strength and elongation. It is reasonable considering that the membranes displayed lower water uptake and swelling ratio from CCPENS-0.2 to CCPENS-0.6 (Fig. 2). Water molecule could act as a plasticizer and weaken the mechanical properties of the AEMs.[52]

Thermogravimetric analysis (TGA) was conducted under N_2 to evaluate the thermal stability of **CCPENS-*x*** AEMs. As shown in Fig. 7, **CCPENS-*x*** all experienced three degradation stages: (1) the 1st small weight loss between 30 and 190 °C was related to the evaporation of residual absorbed water and bound water. (2) the 2nd step from 190 to 410 °C was attributed to the cleavage of C–N bond and decomposition of DIm groups. (3) the 3rd step above 410 °C was owing to the degradation of polymer main chains. In general, all of **CCPENS-*x*** membranes showed good thermal stability below 190 °C. Furthermore, the 5% weight decomposition temperatures ($T_{d\text{-}5\%}$) of **CCPENS-*x*** were increased with increasing the nitrile content (Table 2), which

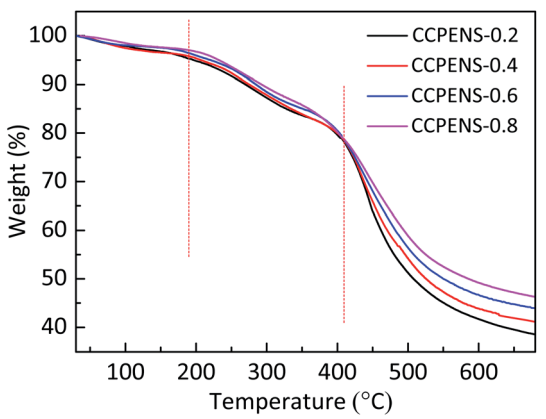

Fig. 7 TGA curves of CCPENS-*x* AEMs.

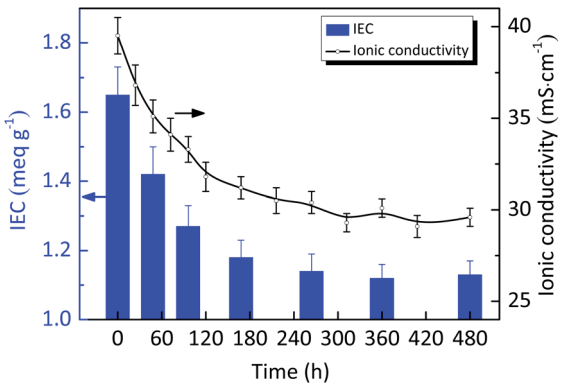

Fig. 8 Alkaline stability of CCPENS-0.8 in a 1 M KOH solution at 80 °C.

might be ascribed to the enhanced intra/intermolecular interaction and indicates the nitrile groups could improve the thermal stability of the AEMs.[53]

Alkaline stability

We assessed the alkaline stability of as-prepared AEMs by monitoring the changes in ionic conductivity and IEC of CCPENS-0.8, which were immersed in a 1 M KOH solution at 80 °C. As shown in Fig. 8, after alkaline treatment of 480 h, CCPENS-0.8 membrane can maintain ~75% (29.6 mS cm^{-1}) of the initial conductivity. Meanwhile, the IEC correspondingly decreased from 1.65 to 1.13 meq. g^{-1}. These could be due to the decomposition of imidazolium functional groups under alkaline environments.[54,55] Fortunately, there are still some means to further improve the alkaline stability of as-prepared AEMs. For example, AEMs prepared by using quinuclidinium or piperidinium cations have been reported for superior alkaline stability.[56,57] These researches inspire us to further enhance the alkaline stability of **CCPENS-*x*** membranes.

Comparison of the present membranes with literature data

A comparison of membrane property between **CCPENS-*x*** and the AEMs reported in recent years is presented in Table S1 (ESI).† As observed, performance of the **CCPENS-*x*** AEMs is in good agreement with other researcher and shows good advantages in anti-swelling.

Conclusions

A series of comb-shaped cardo poly(arylene ether nitrile sulfone) (**CCPENS-*x***) AEMs bearing imidazolium groups on C10 long alkyl side chains was prepared by varying the content of nitrile groups. The IEC of the AEMs ranged from 1.56 to 1.65 meq. g^{-1}. The content of nitrile groups has a significant impact on the morphology and properties of **CCPENS-*x*** AEMs. With the nitrile group content increased, the WU decreased from 24.2% to 21.9% at 30 °C and 35.8% to 27.1% at 80 °C, and the corresponding SR decreased from 7.8% to 6.8% at 30 °C and from 12.7% to 9.2% at 80 °C. Furthermore, **CCPENS-*x*** revealed larger and more interconnected ionic domains to form more efficient ion-transport channels from CCPENS-0.2 to CCPENS-0.8, and the corresponding ionic conductivity increased from 25.8 to 39.5 mS cm^{-1} at 30 °C and 58.6 to 83 mS cm^{-1} at 80 °C. Moreover, **CCPENS-*x*** with higher content of nitrile groups also exhibited better mechanical properties and thermal stability, and higher ratios of conductivity to swelling ratio at 80 °C. Further work will focus on the optimization of membrane alkaline stability.

Conflicts of interest

There are no conflicts to declare.

Acknowledgements

The authors gratefully acknowledge the National Natural Science Foundation of China [No. 21706032], the Young and Middle-aged Teachers Education Scientific Research Project of Fujian Province of China [No. JAT170378], and the Scientific Research Foundation of Huaqiao University (No. 605-50Y18020) for financial support.

Notes and references

1 Z. F. Pan, L. An, T. S. Zhao and Z. K. Tang, *Prog. Energy Combust. Sci.*, 2018, **66**, 141–175.
2 Y. Chang, Y. Qin, Y. Yin, J. Zhang and X. Li, *Appl. Energy*, 2018, **230**, 643–662.
3 G. Merle, M. Wessling and K. Nijmeijer, *J. Membr. Sci.*, 2011, **377**, 1–35.
4 J. Chen, C. Li, J. Wang, L. Li and Z. Wei, *J. Mater. Chem. A*, 2017, **5**, 6318–6327.
5 W. Huang, H. Zhong, D. Li, P. Tang and Y. Feng, *Electrochim. Acta*, 2015, **173**, 575–580.
6 W. Sheng, A. P. Bivens, M. Myint, Z. Zhuang, R. V. Forest, Q. Fang, J. G. Chen and Y. Yan, *Energy Environ. Sci.*, 2014, **7**, 1719–1724.
7 P. Moni, M. G. Pollachini, M. Wilhelm, J. Lorenz, C. Harms, M. M. Murshed and K. Rezwan, *ACS Appl. Energy Mater.*, 2019, **2**, 6078–6086.
8 S. Gottesfeld, D. R. Dekel, M. Page, C. Bae, Y. Yan, P. Zelenay and Y. S. Kim, *J. Power Sources*, 2018, **375**, 170–184.
9 J. R. Varcoe, P. Atanassov, D. R. Dekel, A. M. Herring, M. A. Hickner, P. A. Kohl, A. R. Kucernak, W. E. Mustain, K. Nijmeijer, K. Scott, T. Xu and L. Zhuang, *Energy Environ. Sci.*, 2014, **7**, 3135–3191.
10 M. A. Shehzad, X. Liang, A. Yasmin, X. Ge, X. Xiao, Y. Zhu, Z. Ge, Y. Wang, L. Wu and T. Xu, *J. Mater. Chem. A*, 2019, **7**, 10030–10040.
11 X. Chu, Y. Shi, L. Liu, Y. Huang and N. Li, *J. Mater. Chem. A*, 2019, **7**, 7717–7727.
12 L. Wang and M. A. Hickner, *Soft Matter*, 2016, **12**, 5359–5371.
13 J. R. Nykaza, Y. Ye, R. L. Nelson, A. C. Jackson, F. L. Beyer, E. M. Davis, K. Page, S. Sharick, K. I. Winey and Y. A. Elabd, *Soft Matter*, 2016, **12**, 1133–1144.
14 B. H. Oh, A. R. Kim and D. J. Yoo, *Int. J. Hydrogen Energy*, 2019, **44**, 4281–4292.

15 M. Zhang, C. Shan, L. Liu, J. Liao, Q. Chen, M. Zhu, Y. Wang, L. An and N. Li, *ACS Appl. Mater. Interfaces*, 2016, **8**, 23321–23330.
16 X. Li, Q. Liu, Y. Yu and Y. Meng, *J. Mater. Chem. A*, 2013, **1**, 4324–4335.
17 K. H. Lee, D. H. Cho, Y. M. Kim, S. J. Moon, J. G. Seong, D. W. Shin, J. Y. Sohn, J. F. Kim and Y. M. Lee, *Energy Environ. Sci.*, 2017, **10**, 275–285.
18 X. Dong, D. Lv, J. Zheng, B. Xue, W. Bi, S. Li and S. Zhang, *J. Membr. Sci.*, 2017, **535**, 301–311.
19 K. Yoshimura, Y. Zhao, A. Hiroki, Y. Kishiyama, H. Shishitani, S. Yamaguchi, H. Tanaka, S. Koizumi, J. E. Houston, A. Radulescu, M. S. Appavou, D. Richterf and Y. Maekawa, *Soft Matter*, 2018, **14**, 9118–9131.
20 B. Xue, Q. Wang, J. Zheng, S. Li and S. Zhang, *J. Membr. Sci.*, 2020, **601**, 117923.
21 S. Kim, S. Yang and D. Kim, *Int. J. Hydrogen Energy*, 2017, **42**, 12496–12506.
22 C. G. Morandi, R. Peach, H. M. Krieg and J. Kerres, *J. Mater. Chem. A*, 2015, **3**, 1110–1120.
23 R. Ren, S. Zhang, H. A. Miller, F. Vizza, J. R. Varcoe and Q. He, *ACS Appl. Energy Mater.*, 2019, **2**, 4576–4581.
24 D. Yao, T. Wei, L. Shang, H. Na and C. Zhao, *RSC Adv.*, 2019, **9**, 7975–7983.
25 P. Papakonstantinou and V. Deimede, *RSC Adv.*, 2016, **6**, 114329–114343.
26 M. T. Kwasny and G. N. Tew, *J. Mater. Chem. A*, 2017, **5**, 1400–1405.
27 X. Li, Q. Liu, Y. Yu and Y. Meng, *J. Membr. Sci.*, 2014, **467**, 1–12.
28 D. Shin, A. F. Nugraha, F. Wijaya, S. Lee, E. Kim, J. Choi, H. J. Kim and B. Bae, *RSC Adv.*, 2019, **9**, 21106–21115.
29 M. Zhu, M. Zhang, Q. Chen, Y. Su, Z. Zhang, L. Liu, Y. Wang, L. An and N. Li, *Polym. Chem.*, 2017, **8**, 2074–2086.
30 X. Zhang, S. Li, P. Chen, J. Fang, Q. Shi, Q. Weng, X. Luo, X. Chen and Z. An, *Int. J. Hydrogen Energy*, 2018, **43**, 3716–3730.
31 S. Kwon, A. H. N. Rao and T. H Kim, *J. Power Sources*, 2018, **375**, 421–432.
32 F. Gong, R. Wang, X. Chen, P. Chen, Z. An and S. Zhang, *Polym. Chem.*, 2017, **8**, 4207–4219.
33 Y. Zhu, L. Ding, X. Liang, M. A. Shehzad, L. Wang, X. Ge, Y. He, L. Wu, J. R. Varcoe and T. Xu, *Energy Environ. Sci.*, 2018, **11**, 3472–3479.
34 Z. Zhang, X. Xiao, X. Yan, X. Liang and L. Wu, *J. Membr. Sci.*, 2019, **574**, 205–211.
35 B. Shen and H. Pu, *Int. J. Hydrogen Energy*, 2019, **44**, 11057–11065.
36 D. Koronka, A. Matsumoto, K. Otsuji and K. Miyatake, *RSC Adv.*, 2019, **9**, 37391–37402.
37 L. Liu, X. Chu, J. Liao, Y. Huang, Y. Li, Z. Ge, M. A. Hickner and N. Li, *Energy Environ. Sci.*, 2018, **11**, 435–446.
38 A. H. N. Rao, S. Y. Nam and T. H. Kim, *RSC Adv.*, 2016, **6**, 16168–16176.
39 Y. He, J. Si, L. Wu, S. Chen, Y. Zhu, J. Pan, X. Ge, Z. Yang and T. Xu, *J. Membr. Sci.*, 2016, **515**, 189–195.
40 X. L. Gao, Q. Yang, H. Y. Wu, Q. H. Sun, Z. Y. Zhu, Q. G. Zhang, A. M. Zhu and Q. L. Liu, *J. Membr. Sci.*, 2019, **589**, 117247.
41 L. Zeng and T. S. Zhao, *J. Power Sources*, 2016, **303**, 354–362.
42 J. Pan, C. Chen, Y. Li, L. Wang, L. Tan, G. Li, X. Tang, L. Xiao, J. Lu and L. Zhuang, *Energy Environ. Sci.*, 2014, **7**, 354–360.
43 Y. Hu, B. Wang, X. Li, D. Chen and W. Zhang, *J. Power Sources*, 2018, **387**, 33–42.
44 G. Shukla and V. K. Shahi, *ACS Appl. Energy Mater.*, 2018, **1**, 1175–1182.
45 A. N. Lai, L. S. Wang, C. X. Lin, Y. Z. Zhuo, Q. G. Zhang, A. M. Zhu and Q. L. Liu, *ACS Appl. Mater. Interfaces*, 2015, **7**, 8284–8292.
46 D. S. Kim, Y. S. Kim, M. D. Guiver and B. S. Pivovar, *J. Membr. Sci.*, 2008, **321**, 199–208.
47 Y. Huang, J. Liu, P. Zheng, M. Feng, J. Chen and X. Liu, *J. Polym. Res.*, 2016, **23**, 256.
48 M. Feng, T. Cheng, X. Huang, Y. Huang and X. Liu, *RSC Adv.*, 2017, **7**, 2971–2978.
49 Y. S. Kim, D. S. Kim, B. Liu, M. D. Guiver and B. S. Pivovar, *J. Electrochem. Soc.*, 2008, **155**, B21–B26.
50 X. Dong, S. Hou, H. Mao, J. Zheng and S. Zhang, *J. Membr. Sci.*, 2016, **518**, 31–39.
51 J. Zheng, J. Wang, S. Zhang, T. Yuan and H. Yang, *J. Power Sources*, 2014, **245**, 1005–1013.
52 H. N. Dhakal, Z. Y. Zhang and M. O. W. Richardson, *Compos. Sci. Technol.*, 2007, **67**, 1674–1683.
53 M. Guo, B. Liu, S. Guan, L. Li, C. Liu, Y. Zhang and Z. Jiang, *J. Power Sources*, 2010, **195**, 4613–4621.
54 J. Cheng, G. He and F. Zhang, *Int. J. Hydrogen Energy*, 2015, **40**, 7348–7360.
55 H. Wei, Y. Li, S. Wang, G. Tao, T. Wang, S. Cheng, S. Yang and Y. Ding, *J. Membr. Sci.*, 2019, **579**, 219–229.
56 A. Allushi, T. H. Pham, J. S. Olsson and P. Jannasch, *J. Mater. Chem. A*, 2019, **7**, 27164–27174.
57 J. S. Olsson, T. H. Pham and P. Jannasch, *Adv. Funct. Mater.*, 2018, **28**, 1702758.

